Theoretical and experimental study of the excited state dynamics in reverse saturable absorbers using Z-scan technique

S. Venugopal Rao[a*], Suneel Singh[a], B.S.DeCristofano[#] and D. Narayana Rao[a]

[a]School of Physics, University of Hyderabad, Hyderabad - 500 046, India.
[#]US Army Natick R D & E Center, Natick, MA 01760, USA
[*]e-mail : dnrsprs@uohyd.ernet.in

We report here the experimental observations on the nature of the non-linear absorption, over the visible region (450-700 nm), for C_{60}, porphyrin and pthalocyanine. A theoretical study has been carried out using 3-level (S_0, S_1 and S_n) and a more general 5-level (with triplets T_1 and T_n included) models. Excited state dynamics and various photo-physical parameters have been evaluated through the comparison/fitting of the experimental data to the theoretical models. The effect of the triplets and intersystem crossing reveals the broadening of the open aperture z-scan curve. From our theoretical modelling, we could derive both the excited state absorption cross-section and two-photon absorption cross-sections.

1. INTRODUCTION

Over the last few years physicists, chemists and material scientists have shown tremendous interest in materials exhibiting reverse saturable absorption (RSA) for their potential application as optical limiters. Optical limiters are devices that strongly attenuate optical beams at high intensities while exhibiting higher transmittance at low intensities. Such devices are useful for the protection of human eye and optical sensors from intense laser beams. The development of these materials is based on various mechanisms such as free-carrier absorption and refraction in semiconductors [1], optical breakdown-induced scattering [2], thermal refractive beam spreading [3], two-photon absorption [4] and excited state absorption [5] (see article by L.W.Tutt et. al.[6]). Recent studies show very high performance excited state absorption (ESA) or RSA behaviour in C_{60} [7], porphyrins [8], and phthalocyanines [9]. These materials are characterised by their strong excited state absorption compared to ground state absorption. Most of these materials were studied either at 532 nm or 600 nm and the models used to evaluate the photo-physical parameters were based on 4-level (first excited singlet and triplet levels) or 3-level (singlet levels only) models. For fs and ps pulse excitation, triplet level contribution to the non-linear absorption can be neglected due to slower inter system crossing. Whereas, with ns pulses the triplet levels do play an important role. Depending on the pump intensity and wavelength, the absorption could be (1) from ground state S_0 to the first excited singlet state S_1 and then to T_1 state through inter-system crossing (saturation of absorption) (2) directly from S_0 to S_n states (two-photon absorption) (3) from first excited singlet sate S_1 to higher excited states S_n (ESA/RSA) (4) from T_1 to T_n states (ESA/RSA). One has to incorporate all these absorption phenomena in rate equations in order to obtain exact contribution from each of these processes.
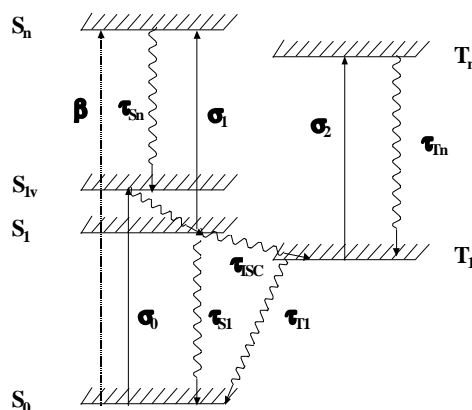

Fig.1 Five-level model used for the study.

We have performed open aperture z-scan of C_{60} (in toluene), porphyrin (THF), and phthalocyanine (Conc. H_2SO_4) in the visible region from 440 nm to 660 nm. To fit our experimental data we consider a theoretical model where contribution to the non-linear absorption could be from S_0 to S_n states (due to direct TPA), S_1 to S_n states (due to ESA/RSA) or T_1 to T_n states (due to ESA/RSA). Different curves are theoretically obtained by varying the parameters: excited state absorption, two-photon absorption and input intensity. The behaviour of the open aperture z-scan curve with changes in the above parameters is discussed in detail.

1. EXPERIMENT

We employ a commercial OPO (MOPO, laser by Spectra Physics) pumped by the third harmonic (355 nm) from the Quanta Ray Nd:YAG laser with a repetition rate of 10 Hz and tunable in the range of 380-1000 nm. The pulse duration of the laser is 6 ns and an aperture of 1.4 mm is used at the output of the MOPO laser to obtain a smooth profile in the far field. The energy after the aperture was varied from 0.2 mJ to 2 mJ/pulse depending on the wavelength. The focal length of the lens used is 50 mm and 1 mm glass cuvettes are used for the solutions (fig. 2). C_{60} (> 99% pure) was brought from Strem Chemicals, USA and dissolved in toluene to make ~ $10^{-4} – 10^{-3}$ M solutions. Copper pthalocyanine (CuPc) was dissolved in concentrated sulfuric acid (10^{-4} M) and tetrabenzporphyrin (ZnmpTBP) was dissolved in THF (10^{-3} M). The values of beam waist at focus are ~ 30-50 μ, the corresponding peak intensities are ~ 10^8 to 10^9 W/cm^2, and the Rayleigh ranges are ~ 6.5 mm to 8 mm depending on the wavelength and the input energy.
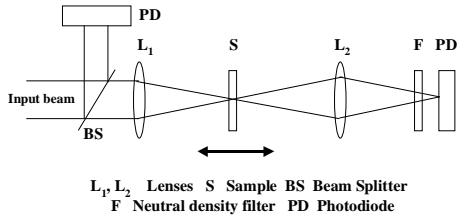

L$_1$, L$_2$ Lenses S Sample BS Beam Splitter
F Neutral density filter PD Photodiode

Fig. 2 Experimental setup.

2. NUMERICAL SIMULATIONS

Rate equations for the five level model shown in fig.2 (where S_0, S_1, S_n, T_1, T_n are approximated to one single level each neglecting the vibrational levels in each maniflod) are :

$$\frac{dN_0}{dt} = -\frac{\sigma_0 I N_0}{\hbar\omega} - \frac{\beta I^2}{2\hbar\omega} + \frac{N_1}{\tau_1} + \frac{N_3}{\tau_4} \tag{1}$$

$$\frac{dN_1}{dt} = -\frac{\sigma_1 I N_1}{\hbar\omega} + \frac{\sigma_0 I N_0}{\hbar\omega} - \frac{N_1}{\tau_1} - \frac{N_1}{\tau_{ISC}} + \frac{N_2}{\tau_2} \tag{2}$$

$$\frac{dN_2}{dt} = \frac{\sigma_1 I N_1}{\hbar\omega} + \frac{\beta I^2}{2\hbar\omega} - \frac{N_2}{\tau_2} \tag{3}$$

$$\frac{dN_3}{dt} = -\frac{\sigma_2 I N_3}{\hbar\omega} - \frac{N_3}{\tau_4} + \frac{N_1}{\tau_{ISC}} + \frac{N_4}{\tau_3} \tag{4}$$

$$\frac{dN_4}{dt} = \frac{\sigma_2 I N_3}{\hbar\omega} - \frac{N_4}{\tau_3} \tag{5}$$

and the intensity transmitted through the sample is given by

$$\frac{dI}{dz} = -\sigma_0 I N_0 - \sigma_1 I N_1 - \sigma_2 I N_3 - \beta I^2 \tag{6}$$

with

$$I = I_{00} * (\frac{\omega_0^2}{\omega^2(z)}) * \exp(\frac{-t^2}{\tau_p^2}) * \exp(\frac{2*r^2}{\omega^2(z)}) \tag{7}$$

and

$$\omega(z) = \omega_0 \left\{ 1 + \left(\frac{z}{z_0} \right)^2 \right\}^{\frac{1}{2}} ; z_0 = \frac{\pi * \omega_0^2}{\lambda}$$

where σ_0 is the ground state absorption cross-section, σ_1 and σ_2 are the excited state absorption cross-sections from S_1 and T_1 states respectively, N_i's are the corresponding populations in the different states, τ_i's are the lifetimes of the excited states, z_0 is the Rayleigh range, ω_0 is the beam waist at focus, I is intensity as a function of r, t, and z, I_{00} is peak intensity at the focus of the gaussian beam, and τ_p is the input pulse width used, β is the two-photon cross-section, and τ_{ISC} is the intersystem crossing rate.

The differential equations are solved numerically using Runge-Kutta fourth order method. The differential equations are first de-coupled and then integrated over time, length, and along the radial direction. Assuming the input beam to be a gaussian, the limits of

integration for r, t, z varied from 0 to ∞, -∞ to ∞, and 0 to L (length of the sample). Typical number of slices used for r, t, z are 60, 30, and 5 respectively. The experimental data is fitted through least square fit method and the excited state absorption coefficient and two-photon absorption coefficients are calculated from the fits.
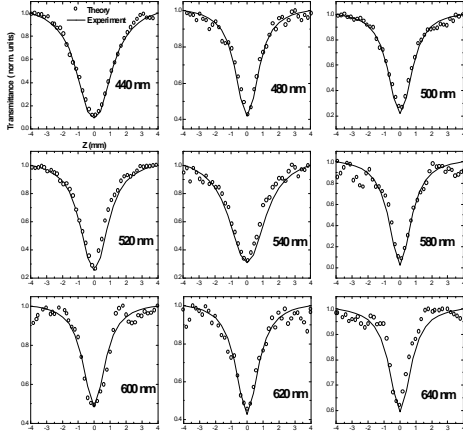

Fig.3 Experimental and theoretical results obtained in C_{60}

Fig.3 shows the experimental data (scattered points) and the theoretical fits (solid lines) obtained using the five level model for wavelengths ranging from 440 nm to 640 nm for the sample C_{60}. Ground state absorption cross-sections for different wavelengths are calculated using $\sigma_0 = (\alpha/N)$ where α is the linear absorption and N is the density of molecules per cm^3. Depending on the wavelength, I_{00} is taken as $\sim 10^8$ to 10^9 W/cm^2, $\omega_0 \sim 30$ to 50 μm, $z_0 \sim 6.5$ to 8 mm. For C_{60}, the relaxation time of the first excited singlet state τ_{S1}, intersystem crossing τ_{ISC}, and the lifetime of the first excited triplet state τ_{T1} are taken as 70 ps, 650 ps, and 280 μs respectively. The relaxation times of S_n and T_n states are taken $\sim$ 100 fs. Excitation wavelengths are indicated for each z-scan curve. In the wavelength region from 440 nm to 540 nm, the experimental data fits better with $\beta = 0$ and in the wavelength region 580 nm to 640 nm, β dominates with smaller contribution from σ_2 / σ_1. Effect of σ_1 and τ_{S1} are shown in fig. 4 at two arbitrary wavelengths , one in 440 - 540 nm range and the other in 580 - 640 nm range. Fig. 4 (a) shows the theoretical curves generated at 480 nm for $\sigma_0 = 3.0*10^{-18}$ cm^2, $\sigma_2 = 12.0*10^{-18}$ cm^2, $\beta = 0.0$, $\sigma_1 = 15.0*10^{-18}$ cm^2 (solid line); $\sigma_0 = 3.0*10^{-18}$ cm^2, $\sigma_2 = 12.0*10^{-18}$

cm^2, $\beta = 0.0$, $\sigma_1 = 0.0$ (dotted line). Fig. 4 (b) shows the theoretical curves generated at 600 nm for $\sigma_0 = 1.65*10^{-18}$ cm^2, $\sigma_2 = 6.60*10^{-18}$ cm^2, $\beta = 0.0$, $\sigma_1 = 6.60*10^{-18}$ cm^2 (solid line); $\sigma_0 = 1.65*10^{-18}$ cm^2, $\sigma_2 = 6.60*10^{-18}$ cm^2, $\beta = 0.0$, $\sigma_1 = 0.0$ (dotted line). As we can see, there is very little effect on the open aperture z-scan curves due to σ_1. This is mainly due to the fact that we have taken τ_{S1} to be 70 ps. Lifetimes of S_1 state have been reported to be ~ 100 ps and ~ 1.2 ns by several groups [10-12]. Our studies performed through incoherent laser spectroscopy [13] have shown a lifetime for the S_1 state as 70 ps. We could obtain a reasonably good fit for σ_1 varying from $15*10^{-18}$ cm^2 to $20*10^{-18}$ cm^2 with σ_2 around $12*10^{-18}$ cm^2. Therefore, there could be larger error in the values of σ_1 compared to σ_2. If fs pulses are used for excitation, then we expect the contribution of σ_1 alone to the non-linear absorption as the intersystem crossing would be too slow when compared to the pulse duration. From the fs data, then one can exactly find out the contribution of σ_1. We are in the process of procuring the fs data in the wavelength region of 440 nm to 540 nm, where the ESA plays a dominant role compared to the TPA as discussed below. We also tried to fit the experimental data using 1.2 ns for the lifetime of the S_1 state. We could obtain a good fit only with $\tau_{S1} = 70$ ps.
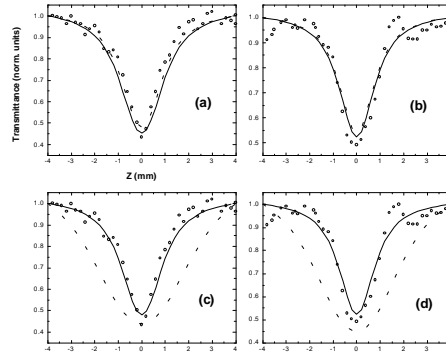

Fig. 4 Theoretical curves generated for $I_{00} = 10^9$ (a) at 480 nm with $\sigma_0 = 3.0*10^{-18}$, $\sigma_2 = 12.0*10^{-18}$, $\beta = 0.0$, $\sigma_1 = 15.0*10^{-18}$ (solid); $\sigma_0 = 3.0*10^{-18}$, $\sigma_2 = 12.0*10^{-18}$, $\beta = 0.0$, $\sigma_1 = 0.0$ (dotted), (b) at 600 nm with $\sigma_0 = 1.65*10^{-18}$, $\sigma_2 = 6.60*10^{-18}$, $\beta = 0.0$, $\sigma_1 = 6.60*10^{-18}$ (solid); $\sigma_0 = 1.65*10^{-18}$, $\sigma_2 = 6.60*10^{-18}$, $\beta = 0.0$, $\sigma_1 = 0.0$ (dotted), (c) at 480 nm with $\sigma_0 = 3.0*10^{-18}$, $\sigma_2 = 12.0*10^{-18}$, $\beta = 0.0$, $\tau_{S1} = 1.2$ ns (solid); $\sigma_0 = 3.0*10^{-18}$, $\sigma_2 = 12.0*10^{-18}$, $\beta = 0.0$, τ_{S1} = 70 ps (dotted), (d) at 600 nm with $\sigma_0 = 1.65*10^{-18}$,

$\sigma_2 = 6.60*10^{-18}$, $\beta = 0.0$, $\tau_{S1} = 1.2$ ns (solid); $\sigma_0 = 1.65*10^{-18}$, $\sigma_2 = 6.60*10^{-18}$, $\beta = 0.0$, $\tau_{S1} = 70$ ps (dotted),. The scattered points are the experimental data, only for comparison.
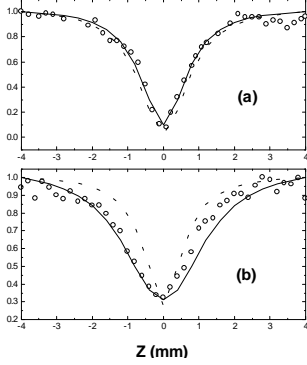

Fig.5 Theoretical curves generated (a) for $I_{00} = 8.6*10^8$ at 540 nm with $\sigma_0 = 2.69*10^{-18}$, $\sigma_1 = 18.2*10^{-18}$, $\sigma_2 = 11.4*10^{-18}$, $\beta = 0.0$ (solid); $\sigma_0 = 2.69*10^{-18}$, $\sigma_1 = 5.0*10^{-18}$, $\sigma_2 = 8.0*10^{-18}$, $\beta = 0.5*10^{-8}$ (dotted), (b) for $I_{00} = 4.6*10^8$ at 580 nm with $\sigma_0 = 1.445*10^{-18}$, $\sigma_2 = 0.0$, $\beta = 2.6*10^{-8}$ (solid); $\sigma_0 = 1.445*10^{-18}$, $\sigma_2 = 3*10^{-18}$, $\beta = 2.45*10^{-8}$ (dotted curve). The scattered points are the experimental data, only for comparison.

Simulated curves for both the time scales are shown in fig.'s 4 (c) for 440 nm and 4 (d) for 600 nm (dotted line is the curve with $\tau_{S1} = 1.2$ ns and solid line is the curve with $\tau_{S1} = 70$ ps with all other parameters remaining the same). We clearly see that for $\tau_{S1} = 1.2$ ns, the curves become very broad indicating that for the C_{60} sample, that has been used in our system, $\tau_{S1} = 70$ ps. The present results are therefore consistent with our earlier studies reported through DFWM experiments done with a broad band laser [13]. The sample that has been used in both the experiments is from the same batch and company.

λ (nm)	σ_0 (10^{-18}) (cm^2)	σ_1 (10^{-18}) (cm^2)	σ_2 (10^{-18}) (cm^2)	β (cm/GW)
440	1.79	22.0	14.0	-
480	2.99	12.8	9.6	-
500	2.69	14.8	11.6	-
520	2.7	22.2	11.4	-
540	2.69	18.2	11.4	-
580	1.445	-	3.0	24.5
600	1.65	-	2.4	22.5
620	1.03	-	3.6	19.5
640	0.724	-	2.2	18.5

Table 1. Values calculated using the 5-level model.

The values of σ_1, σ_2, β are shown in table 1. There is no contribution from TPA (β) to the non-linear absorption till 540 nm. From 580 nm to 640 nm the non-linear absorption is mainly due to two-photon absorption. S_n and S_1 energies of C_{60} fall in the region of ~ 29,000 cm^{-1} and S_1 state falls in ~16000 cm^{-1} range respectively [14]. Excitations longer than 580 nm fall either on the lower edge of the absorption curve or below it. Since at such excitations, it is expected that either the molecule relaxes to the ground state through τ_{S1}, or remains localized in those lower energy levels without diffusion into higher levels [15]. This suggests clearly a direct TPA either through a virtual level or an intermediate level. We have tried to fit the data in this region with $\sigma_2 = 0$ (fig. 5 (a) solid line) and also by introducing non-zero value of σ_2 (fig. 5 (a) dotted line). Even though both the fits are close to the experimental data, the curve with β alone having lower value of chisquare among the two, we have fitted the data for β as well as σ. However, we clearly see the domination of TPA in this wavelength region. A complete reversal in the domination of σ_2 and β are observed in the regions below 580 nm as can be seen from their values. In the region above 580 nm, σ_2 falls to $3*10^{-18}$ cm^2, compared to its value of ~ $12*10^{-18}$ cm^2 in the shorter wavelength region. Whereas introduction of small value of β leads to a sharper valley below 580 nm (fig. 5 (b) solid line is obtained without β and dotted line with β) deviating from the experimental values.

Comparing the values obtained from our modelling with those reported in literature, Kost et. al. working with 532 nm, 8 ns pulses report values of σ_0 as $1.21*10^{-18}$ cm^2, $\sigma_1 = 8.07*10^{-18}$ cm^2 and $\sigma_2 = 5.35*10^{-18}$ cm^2. Chunfei Li working with 15 ns pulses at 532 nm report values of σ_0 as $2.87*10^{-18}$ cm^2, $\sigma_1 = 15.7*10^{-18}$ cm^2 and $\sigma_2 = 9.22*10^{-18}$ cm^2 with $\tau_{S1} = 30$ ns, $\tau_{T1} = 280$ μs, $\tau_{ISC} = 1.2$ ns. Barosso et. al. report values of ($\tau_{S1} = 1.3$ ns, $\tau_{T1} > 150$ ns) (a) 308 nm, $\sigma_0 = 5.6*10^{-17}$ cm^2, $\sigma_2 = 9.1*10^{-17}$ cm^2, (b) 337 nm, $\sigma_0 = 1.5*10^{-16}$ cm^2, $\sigma_2 = 9.2*10^{-17}$ cm^2, (c) 534 nm, $\sigma_0 = 3.2*10^{-18}$ cm^2, $\sigma_2 = 1.4*10^{-17}$ cm^2. We obtain a value of $\sigma_0 = 2.7*10^{-18}$ cm^2, $\sigma_1 = 22.2*10^{-18}$ cm^2, $\sigma_2 = 11.4*10^{-18}$ cm^2 at 520 nm which are close to the values of σ_1 and σ_2 as reported by Kost and

Li, and $\sigma_0 = 2.69*10^{-18}$ cm^2, $\sigma_1 = 18.2*10^{-18}$ cm^2, $\sigma_2 = 11.4*10^{-18}$ cm^2 at 540 nm. However as τ_{S1} is 70 ps and τ_{ISC} is 650 ps, the contribution to σ is predominantly from the triplet population compared to singlet population. Bezel et. al. [16] report two-photon absorption coefficient β at 612 nm (using fs pulses) as $\leq (3 \pm 1.5)*10^{-8}$ cm/W. McBranch et. al. reports β_{eff} values at 561 nm as $0.96*10^{-8}$ cm/W, at 575 nm as $1.85*10^{-8}$ cm/W and at 680 nm as $0.18*10^{-8}$ cm/W. Couris et. al. reports β_{eff} values of $3.9*10^{-8}$ cm/W, $3.14*10^{-8}$ cm/W, $1.91*10^{-8}$ cm/W at 620 nm, 630 nm, 640 nm respectively. We obtain values of $2.25*10^{-8}$ cm/W, $1.95*10^{-8}$cm/W, $1.85*10^{-8}$ cm/W at 600 nm, 620 nm and 640 nm respectively which is in good agreement with those reported by Couris et. al.
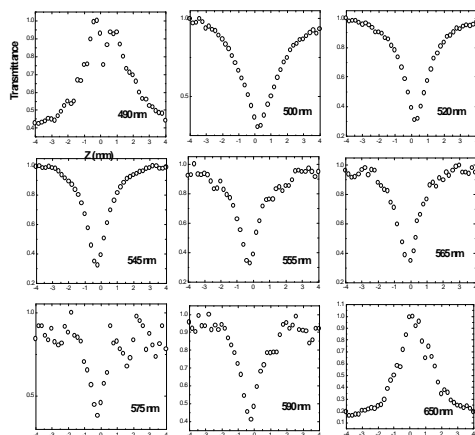

Fig.6 Experimental results obtained for ZnmpTBP (THF) Solution

Fig.'s 6 and 7 show the experimental results obtained for ZnmpTBP and CuPc. For TBP the nonlinear absorption is saturated in the lower wavelength region (490 nm) and also at the high wavelength region (660 nm). In the other regions we can clearly see reverse saturable absorption (either ESA or TPA). Similarly for CuPc we observe saturation of absorption in the 460 nm range and RSA (either ESA or TPA) in the rest of the wavelength region. The theoretical fitting is in progress for these compounds and the results will be presented.
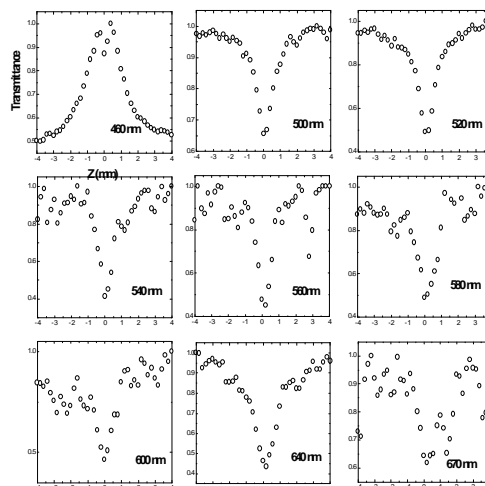

Fig. 7 Experimental results obtained for CuPc (H$_2$SO$_4$) solution.

3. CONCLUSIONS

In conclusion we have studied the dispersion behaviour of non-linear absorption in C$_{60}$, porphyrin, and a phthalocyanine using open aperture z-scan. We have fitted our data using a 5-level model taking into account both the non-linear absorption processes, ESA and TPA. We have derived the information about the non-linear absorption processes from the shape of the open aperture z-scan curves. The main advantage of the C$_{60}$, in comparison to porphyrins and phthalocyanines, is that it shows RSA behaviour over the entire visible region, either through ESA in the shorter wavelengths or through TPA in the longer wavelength region.

5. REFERENCES

1. E.W.Vanstryland, Y.Y.Wu, D.J.Hagan, M.J.Soileau, J. Opt. Soc. Am. **B5**, 1988, 1980.
2. K.Mansour, M.J.Soileau, E.W.Vanstryland, J. Opt. Soc. Am. **B9**, 1992, 1100.
3. B.L.Justus, A.J.Campillo, A.L.Huston, Opt. Lett., **19**, 1994, 693.
4. Guang S. He, Raz Gvishi, Paras N. Prasad, Bruce A. Rinhardt, Opt. Commun., **117**, 1995, 133; Guang S. He, Gen C. Xu, Paras N. Prasad, Bruce A. Reinhardt, Jay C. Bhatt, and Ann G. Dillard, Opt. Lett., **20**, 1995, 435; Guang S. He, Jayanat D. Bhawalkar, Chan F. Zhao, and Paras N. Prasad, Appl. Phys. Lett., **67**, 1995, 2433.
5. L.W.Tutt and A.Kost, Nature, **356**, 1992, 225.
6. L.W.Tutt and T.F.Bogges, Prog. Quant. Elcetr., **17**, 1993, 299.
7. V.V. Govlev, W.R.Garrett, and C.H.Chen, J. Opt. Soc. Am. **B13**, 1996, 2801; C.Li, L.Zhang, R.Wang, Y.Song, Y.Wang, J. Opt. Soc. Am. **B11**, 1994, 1356; Denis Vincent and James Cruickshank, Applied Optics, **36**, 1997, 7794; Y.A.-Ping Sun, Jason E. Riggs, and Bing Liu, Chem. Mater., **9**, 1997, 1268; D.McBranch, B.R.Mattes, A.Koskelo, J.M.Robinson, and S.P.Love, SPIE Proc., **2284**, 1994, 15; D.MCBranch, L.Smilowitz, V.Klimov, A.Koskelo, J.M.Robinson, B.R.Mattes, J.C.Hummelen, F.Wudl, J.C.Withers, and N.F.Borrelli, SPIE Proc., **2530**, 1995, 196; S.R.Mishra, H.S.Rawat, and S.C.Mehendale, Appl. Phys. Lett., **71**, 1997, 46; S.R.Mishra, H.S.Rawat, M.P.Joshi and S.C.Mehendale, J. Phys. B: At. Mol. Phys., **27**, 1994, L157; S.R.Mishra, H.S.Rawat, M.P.Joshi and S.C.Mehendale, Appl. Phys. **A63**, 1996, 223.
8. W.Blau, H.Byrne, W.H.Dennis, J.M.Kelly, Opt. Commun., **56**, 1985, 25; S.Guha, K.Kong, P.Porter, J.F.Roach, D.E.Remy, F.J.Aranda, D.V.G.L.N.Rao, Opt. Lett., **17**, 1992, 264; J.Si, M.Yang, Y.Wang, L.Zhang, C.Li, D.Wang, S.Dong, W.Sun, Appl. Phys. Lett., **64,** 1994, 3083.
9. J.W.Perry, K.Mansour, I.-Y.S.Lee, X.-L.Wu, P.V.Bedworth, C.-T.Chen, D.Ng, S.R.Mardar, P.Miles, T.Wada, M.Tran, H.Sasabe, Science, **273**, 1996, 1553; J.S.Shirk, R.G.S.Pong, F.J.Bartoli, A.W.Snow, Appl. Phys. Lett. **63**, 1993, 1880; J.W.Perry et. al. Opt. Lett., **19**, 1994, 625; T.H.Wei, D.J.Hagan, M.J.Sence, E.W.Vanstryland, J.W.Perry, D.R.Coulter, Appl. Phys. **B54**, 1992, 46; C.Li, L.Zhang, M.Yang, H.Wang, Y.Wang, Phys. Rev. **A49**, 1994, 1149.
10. R.A.Cheville and N.J.Halas, Phys. Rev. **B45**, 1992, 4548; V.M.Farztdinov, Y.E.Lozovik, Y.A.Matveets, A.G.Stepanov, and V.S.Letokhov, J. Phys. Chem., **98**, 1994, 3290; I.E.Kardash, V.S.Letokhov, Y.E.Lozovik, Y.A.Matveets, A.G.Stepanov, and V.M.Farztdinov, JETP Lett., **58**, 1993, 138.
11. S.B.Fleischer, E.P.Ippen, G.Dresselhaus, M.S.Dresselhaus, A.M.Rao, P.Zhou, and P.C.Elkund, Appl. Phys. Lett., **63**, 1993, 3241; T.W. Ebbesen, K.Tanigaki, and S.Kuroshima, Chem. Phys. Lett., **181**, 1991, 501.
12. R.J.Sension, C.M.Phillips, A.Z.Szarka, W.J.Romanow, A.R.McGhie, J.P.McCauley, Jr., A.B.Smith III, and M.Hochstrasser., J. Phys. Chem., **95**, 1991, 6075; M.R.Wasielewski, M.P.O'Neil, K.R.Lykke, M.J.Pellin, and D.M.Gruen, J. Am. Chem. Soc., **113**, 1991, 2774.
13. S.Venugopal Rao and D.Narayana Rao, Chem. Phys. Lett., **283**, 1998, 227.
14. Minyung Lee, Ok-Keun Song, Jung-Chul Seo, Dongho Kim, Yung Dung Suh, Seung Min Jin and Seong Keun Kim, Chem. Phys. Lett., **196**, 1992, 325.
15. G.B.Talapatra, D.Narayana Rao, and Paras N. Prasad, J. Phys. Chem., **88**, 1984, 4636.
16. I.V.Bezel, S.V.Chekalin, Yu.A.Matveets, A.G.Stepanov, A.P.Yartsev and V.S.Letokhov, Chem. Phys. Lett., **218**, 1994, 475.